ISBN: 978-3-95450-227-1 ISSN: 2673-5490 doi:10.18429/JACoW-IPAC2022-WEOXSP3

mm-WAVE STRUCTURE DEVELOPMENT FOR HIGH GRADIENT ACCELERATION*

E. C. Snively†, A. Gabriel, M. A. K. Othman, A. Sy, E. A. Nanni,
SLAC National Accelerator Laboratory, Menlo Park, U. S. A.

Abstract

We report on the design of high shunt impedance accelerator structures operating near 100 GHz. Simulations of the cavity geometry and RF coupling are performed in ANSYS-HFSS and using SLAC's parallel electromagnetic code suite ACE3P. We present experimental results for structures fabricated from copper, niobium, and copper plated with NbTiNi. We report on techniques for tuning these high frequency structures. A mm-wave accelerator cavity enables not only a high achievable gradient due to higher breakdown thresholds, but also reduced fill times which decrease pulsed heating and allow for higher repetition rates.

INTRODUCTION

Accelerators operating in the mm-wave regime offer an attractive opportunity to reach accelerating gradients of hundreds of MeV/m and repetition rates exceeding 1 kHz. Recent research exploring the high gradient performance and breakdown statistics of mm-wave structures has demonstrated gradients up to 225 MeV/m [1,2]. The cavity geometry in this case was designed to match X-band cavities used in previous experiments, allowing direct comparison of the breakdown statistics collected in both frequency regimes [3,4]. The research presented here builds on this foundation of high-power mm-wave tests with measurements of cavities matching the first-generation geometry, along with a second-generation cavity geometry for higher shunt impedance. The challenge of extending the mm-wave structure is met with a side-coupled cell design for a distributed power coupling manifold [5]. Tuning techniques adapted for the mm-wave regime are tested with first-generation cavities.

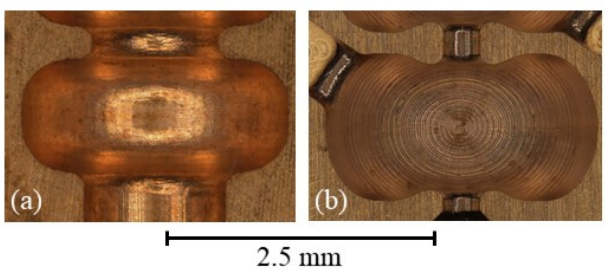

Figure 1: (a) Microscope image of a "first-generation" mm-wave cavity (110 GHz) with power coupling on-axis. (b) Microscope image of a "second-generation" cavity (94 GHz) with re-entrant nose cones and side power coupling.

* Work supported by U.S. Department of Energy Contract No. DE-AC02-76SF00515, SLAC LDRD project 21-014 and Internal Agency Agreement 21-0007-IA (MIPR HR0011150657).

† esnively@slac.stanford.edu

ACCELERATOR DESIGN

A key difference between the first-gen and second-gen cavity design is the approach to power coupling. Figure 1 shows microscope images of fabricated cavities of each type. Both structures are π-mode standing wave cavities resonant near 100 GHz. The first-gen cavity has large iris apertures which facilitate power coupling on-axis; the second-gen cavity has a side-coupled power feed and small iris apertures (330 μm) with reentrant nose cones. Measurements taken with a Vector Network Analyzer (VNA) to characterize the first-gen structures must rely on coaxial probes aligned within the beam pipe. Measurements of the second-gen structure use WR-10 waveguide connections routed to each cavity as shown in Fig. 2a. The re-entrant nose cones and small iris apertures enable a high shunt impedance, around 440 MΩ/m, while significantly reducing coupling between cells as shown in the HFSS simulations of the field profiles in Figure 2.

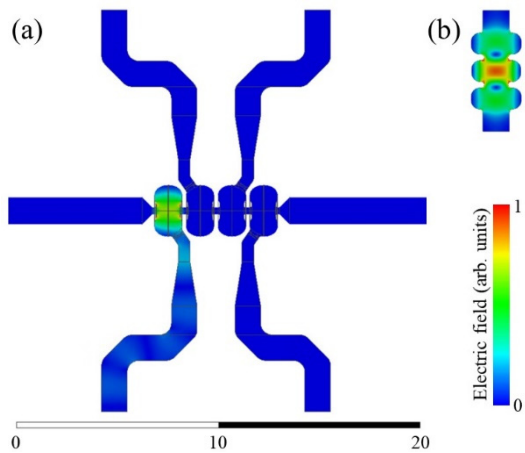

Figure 2: (a) HFSS simulation of the 4-cell side-coupled second-gen prototype with power driven at 93.9 GHz into the first cell. (b) HFSS simulation of the 3-cell first-gen design with peak field intensity localized in the central cell.

The length-scale of mm-wave structure fabrication pushes the limits of conventional machining technology. To test the feasibility of fabricating the second-gen cavity geometry with features like the side-coupled waveguide feeds and re-entrant nose cones, the four-cell prototype geometry shown in Fig. 2a was designed. Machining tolerances for the re-entrant nose cone feature were informed by the results of a mm-wave cavity design study for a beam driven power extractor [6]. The waveguide routing of the 4-cell second-gen cavity prototype allows for the characterization of each cell individually, without the added complexity of a power distribution manifold that would require

ISBN: 978-3-95450-227-1 ISSN: 2673-5490 doi:10.18429/JACoW-IPAC2022-WEOXSP3

shorting neighbouring cells. The WR-10 waveguide connections greatly improve the simplicity and reproducibility of the cold test procedure, as compared to the coaxial probe method used on the first-gen structures.

COLD TEST AND TUNING RESULTS

Measurements of the transmission coefficient in first-gen structures fabricated out of copper, niobium, and copper plated with NbTiNi are shown in Figure 3. During cold test, the structures were clamped with stainless steel shims between the split-block halves to shift the resonant frequencies down. Three resonances, corresponding to the 0, π/2, and π-modes, are visible in the 3-cell structures. S-parameter measurements of the 4-cell second-gen prototype fabricated from copper are shown in Figure 4. HFSS simulations of the predicted S-parameter values are shown with a dashed pink line. The spread in resonant frequency between the 4 cells is 46 MHz, reaching a maximum of 122 MHz away from the design frequency of 93.99 GHz.

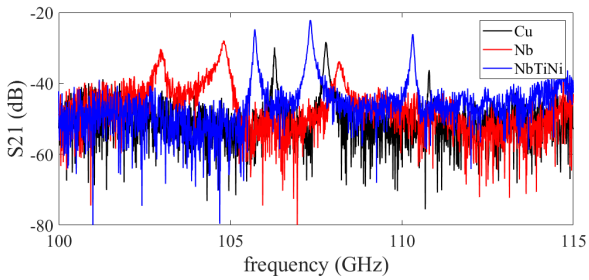

Figure 3: Network analyzer measurement of S_{21} performed using coaxial probes inserted along the beam pipe of 3-cell first-gen structures fabricated from Cu, Nb, and NbTiNi.

The initial tuning approach for the first-gen structures relied on stainless steel shims of variable thickness, producing an overall shift down in the resonant frequencies. Conventional tuning pins brazed to the wall of each cavity would allow targeted tuning of the relative frequency between cavities, but the cell period in a mm-wave structure, roughly 1.6 mm, is too small for this approach. An alternative method to achieve this targeted tuning was developed using a demountable tuning fixture, as shown in Figure 5a.

First-gen prototype structures were modified to allow access to a 1 mm thick cavity wall. The position of the tuning fixture relative to each cell was determined by pairs of mounting holes, offset to accommodate the short period.

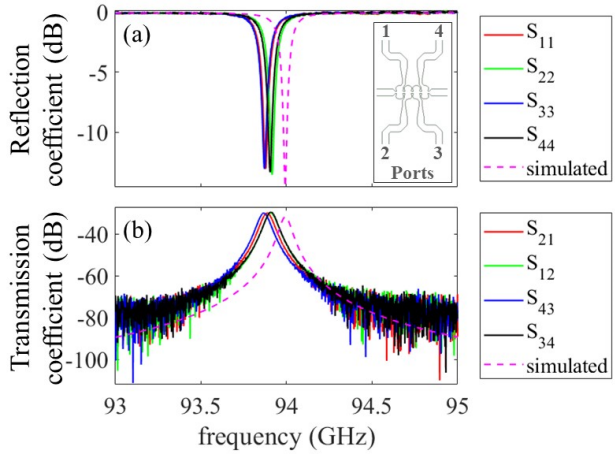

Figure 4: (a) Reflection coefficients at each port of the 4-cell second-gen structure prototype. (b) Transmission coefficients between neighboring cells. The transceiver and receiver were moved to the corresponding ports for each measurement. HFSS simulations of the S-parameters are shown with a dashed pink line.

The resonant frequencies of the 3 modes in the first-gen structure were monitored continuously using coaxial probes. The tuning pin fixture was moved to each cell in sequence. VNA measurement were saved before and after each step in the process as shown in Figure 5c. Because of the strong coupling between cells in the first-gen structure, pressure on the wall of one cell contributes to a frequency shift in all three resonant modes. However, the effect on each mode differs for the 3 cells, resulting in non-uniform shifts during the intermediate steps in the tuning process, see Figure 5d. The measurements shown in Fig. 5 are recorded after the tuning pin fixture was removed from each cavity position. The rebound between the measured resonant frequency while the tuning pin pressed against a cell wall and after it was removed averaged 158 MHz.

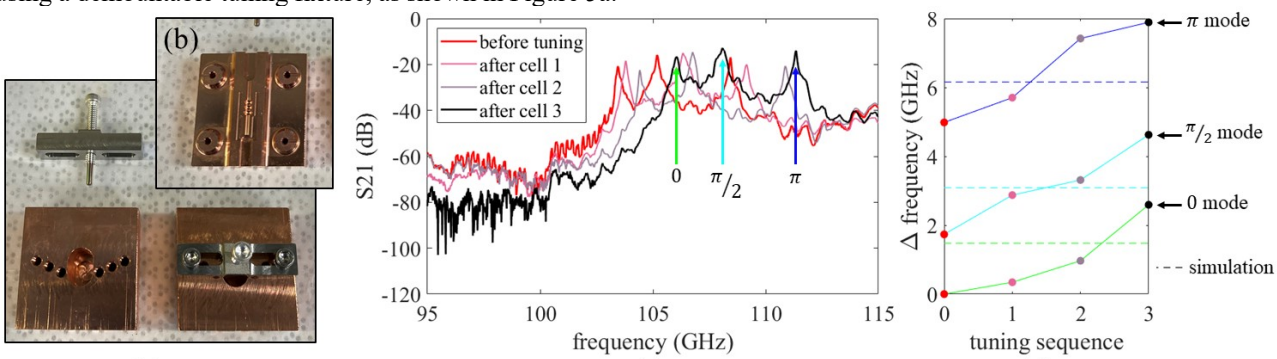

Figure 5: (a) Photograph of the outer surface of split-block halves of a 3-cell linac prototype, modified to allow access with a tuning pin. Tuning fixtures can be attached on both sides with mounting holes determining the cavity targeted by the tuning pin. (b) The inner surface of one half of the slab showing the 3-cell geometry. (c) Network analyzer measurement of S_{21} performed using coaxial probes inserted along the beam pipe during tuning. (d) Plot showing the change in resonant frequency of the 0, π/2, and π-modes in the 3-cell structure after the tuning pin was removed.

ISBN: 978-3-95450-227-1 ISSN: 2673-5490 doi:10.18429/JACoW-IPAC2022-WEOXSP3

The tuning procedure illustrated in Fig. 5 was designed to test the limits of the feasible tuning range with this fixtured tuning pin approach. The measured frequency shift exceeded by more than an order of magnitude the expected tuning range required for a structure matching the fabrication specs of the second-gen prototype measured in Figure 4. Tuning with this fixtured tuning pin approach can only shift the resonant frequencies up. The fabricated second-gen prototype was consistently below the design frequency, suggesting this approach may be sufficient.

A preliminary technique for targeted tuning down in frequency was also investigated. In this case a tuning pin was pressed against the cavity wall from the inside of the structure, leaving a depression as shown in Figure 6a. The significant disadvantage of this approach is that the structure must be disassembled during the modification of the cavity. For this preliminary test, each half of every cell received a pin indentation, resulting in an overall shift in the three resonant frequencies observed in the first-gen structure by an average of 63 MHz. Further study is needed to develop a procedure with the precision and repeatability that would be required for this tuning approach, given that the resonant frequency cannot be actively monitored during tuning. The features produced by the pin indentation will also require additional study to determine whether discontinuities in the surface are generated which may impact rf properties and surface fields under high power testing.

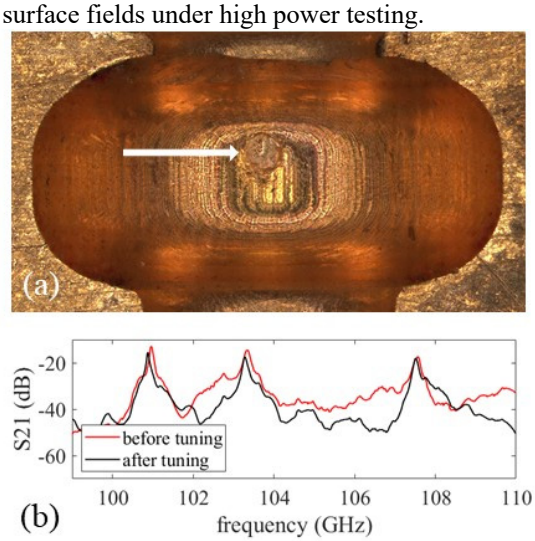

Figure 6: (a) Microscope image of a mm-wave cavity with tuning indent (white arrow) from pin pressed against the inside wall. (b) Network analyzer measurement of S_{21} performed using coaxial probes inserted along the beam pipe of a 3-cell copper structure, before and after pin tuning technique. The π-mode has shifted down by 47 MHz.

DISTRIBUTED COUPLING

To extend the side-coupled cavity geometry to multi-cell structures with efficient power coupling, a distributed waveguide manifold was designed, as shown in Figure 7. Simulations of this 16-cell structure predict up to 3 MeV energy gain for 1 MW of dissipated power. The quasi-optical coupling horn shown if Fig. 7a is adapted from previous high-power tests with the first-gen structures.

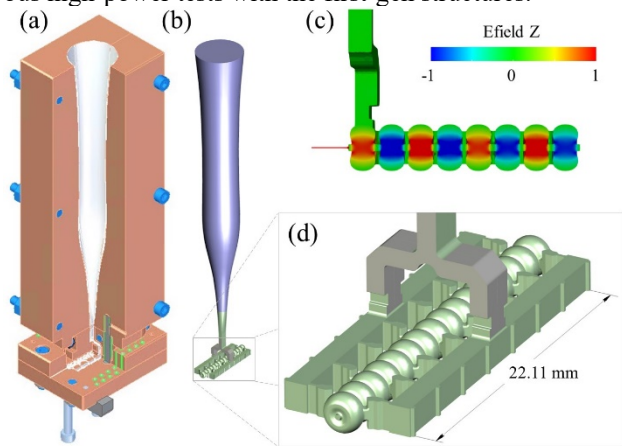

Figure 7: (a) CAD model of the 16-cell distributed coupling linac with quasi-optical coupling horn. (b) Vacuum space of the linac and horn. (c) ACE3P simulation with cutout view of on-axis electric field. (d) View of the linac vacuum space showing power distribution waveguides.

CONCLUSION

The designs presented here establish a method of scaling a mm-wave accelerator cavity to a multi-cell structure that is optimized for maximum shunt impedance. These innovations set the groundwork for high power testing of an extended distributed coupling multi-cell mm-wave accelerator, capable of reaching high gradients with input powers at the level of a MW. The tuning techniques reported here achieve a range more than sufficient to compensate for the frequency variations measured in fabricated prototypes. With continued advances in mm-wave source technology and the development of active pulse gating and compression techniques [7-9], this technology will be poised to enable compact accelerators providing >100 MeV on the sub-meter scale with repetition rates on the order of 1 kHz. This new operating regime will open doors to novel capabilities in a wide range of applications, from advanced radiation therapy techniques, like spatially fractionated high dose rate direct electron therapy, to improved accessibility for accelerator-based discovery science with compact cost-effective high gradient systems.

ACKNOWLEDGEMENTS

The authors would like to thank Zenghai Li, Valery Dolgashev, Sami Tantawi, Muhammad Shumail, Julian Merrick, Samantha Lewis, Andy Haase, Dennis Palmer, Kaitlin Deering, Shirin Kuppusamy, George Wehner, and Mitchell Schneider for many helpful discussions.

This research used resources of the National Energy Research Scientific Computing Center (NERSC), a U.S. Department of Energy Office of Science User Facility operated under Contract No. DE-AC02-05CH11231.

ISBN: 978-3-95450-227-1 ISSN: 2673-5490 doi:10.18429/JACoW-IPAC2022-WEOXSP3

REFERENCES

[1] E. A. Nanni *et al.,* "Results from mm-wave accelerating structure high-gradient tests," In *Proc. 43rd International Conference on Infrared, Millimeter, and Terahertz Waves (IRMMW-THz)*. Nagoya, Japan. Sept. 2018. doi:10.1109/IRMMW_THz.2018.8510478

[2] M. A. K. Othman *et al.*, "Experimental demonstration of externally driven millimeter-wave particle accelerator structure," *Applied Physics Letters,* vol. 117, no. 7, pp. 073502, 2020. doi:10.1063/5.0011397

[3] E.A. Nanni, V.A. Dolgashev, A. Haase, J. Neilson, S. Tantawi, S.C. Schaub, R.J. Temkin and B. Spataro, "Prototyping high-gradient mm-wave accelerating structures", In *Journal of Physics: Conference Series* (Vol. 874, No. 1, p. 012039). July 2017. IOP Publishing.

[4] Dolgashev, Valery, *et al*. "Geometric dependence of radio-frequency breakdown in normal conducting accelerating structures." *Applied Physics Letters* 97.17 (2010): 171501.

[5] S. Tantawi, *et al.,* "Design and demonstration of a distributed-coupling linear accelerator structure," *Phys. Rev. Accel. Beams* vol. 23, no. 9, pp. 092001, 2020. doi:10.1103/PhysRevAccelBeams.23.092001

[6] F. Toufexis *et al.,* "Development of a W-Band Power Extrac-tion Structure," in *Proc. IPAC'19,* Melbourne, Australia. May 2019, pp. 4252-4255. doi:10.18429/JaCoW-IPAC2019-THPTS063

[7] M. Thumm, "State-of-the-Art of High Power Gyro-Devices and Free Electron Masers," *Update in 2016 KIT Scientific Re-ports,* vol. 7735, KIT Scientific Publishing. 2017. doi:10.5445/KSP/1000081551

[8] S. G. Tantawi *et al.,* "Active high-power RF pulse compres-sion using optically switched resonant delay lines," *IEEE transactions on microwave theory and techniques*, vol. 45, no. 8, pp. 1486-1492, 1997. doi:10.1109/22.618460

[9] S. V. Kutsaev *et al.,* "Nanosecond rf-power switch for gyro-tron-driven millimeter-wave accelerators," *Physical Review Applied*, vol. 11, no. 3, pp. 034052, 2019. doi:10.1103/PhysRevApplied.11.034052